A&A 480, L29–L32 (2008)
DOI: 10.1051/0004-6361:20079190

Astronomy & Astrophysics

Letter to the Editor

High-resolution thermal infrared imaging of MWC300

VLT/VISIR observations in BURST mode⋆

A. Domiciano de Souza[1], P. Kervella[2], P. Bendjoya[1], and G. Niccolini[1]

[1] Lab. H. Fizeau, CNRS UMR 6525, Univ. de Nice-Sophia Antipolis, Observatoire de la Côte d'Azur, 06108 Nice Cedex 2, France
e-mail: Armando.Domiciano@unice.fr
[2] LESIA, Observatoire de Paris, CNRS UMR 8109, UPMC, Université Paris Diderot, 5 place Jules Janssen, 92195 Meudon, France

Received 4 December 2007 / Accepted 24 January 2008

ABSTRACT

Context. B[e] stars are expected to possess dusty circumstellar environments, which are responsible for a strong infrared (IR) excess.
Aims. Using single-dish diffraction-limited imaging in the thermal infrared domain, we aim at measuring the angular extension of the dusty environment of the galactic B[e] MWC 300.
Methods. We obtained diffraction-limited images of MWC 300 at 11.25 μm using the BURST mode of the VLT/VISIR instrument.
Results. MWC 300 is partially, but statistically significantly, resolved by VISIR so that we could measure the size of its dusty envelope for the first time. By assuming a 2D circular Gaussian intensity distribution and using different image analysis methods we measured a *FWHM* angular size of 69 ± 10 mas. For a distance of 1.8 kpc, we obtain a linear size of 125 ± 18 AU = (1.87 ± 0.26) × 10^{13} m for the circumstellar dust emitting in the mid-IR. This measured size is shown to agree with a model that was calculated with our radiative radiative transfer code and constrained by previously reported SED data. Additionally, the flux of MWC 300 at 11.25 μm is estimated as 84.5 ± 1.4 Jy = (20.0 ± 0.3) × 10^{-13} W/m^2/μm.
Conclusions. The VLT/VISIR now offers the possibility of obtaining mid-IR diffraction-limited images with a high signal-to-noise ratio. The MWC 300's size as directly measured in this work is compatible with the theoretical size of a nearly edge-on dusty disc estimated in previous works. Interferometric data at milliarcsec angular resolution are required to reveal details on this dusty envelope.

Key words. stars: individual: MWC300 – methods: observational – techniques: high angular resolution – stars: emission-line, Be

1. Introduction

MWC 300 (V431 Sct) is a galactic B[e] star whose classification (Lamers et al. 1998) is not clear yet: is it an evolved supergiant or a Herbig Be star? The supergiant B[e] hypothesis is nevertheless favoured after the work of Miroshnichenko et al. (2004, hereafter M04), who performed an extensive study of MWC 300 based mainly on spectroscopic (UV to near-IR) and photometric data. These authors estimate a distance d = 1.8 ± 0.2 kpc and a luminosity $\log L/L_\odot$ = 5.1 ± 0.1 for MWC 300. M04 also obtained mid-IR images showing that MWC 300 was unresolved at ≃1.″1. This upper limit to the mid-IR size is compatible with their physical modelling, which showed that MWC 300 has a dusty disc seen nearly equator-on with an angular diameter of a few tens of milliarcseconds (mas); in particular, the model inner dust radius is 11 mas.

Interferometric and/or imaging instruments can nowadays attain the required angular resolutions for directly measuring the mid-IR size of MWC 300 and of other B[e] stars in general (e.g., Domiciano de Souza et al. 2007). In this work we use the imaging capabilities of the ESO VLT/VISIR instrument to obtain diffraction-limited images of MWC 300 in the mid-IR (11.25 μm). The observations are described in Sect. 2. The results and conclusions are given in Sects. 3 and 4.

⋆ Based on observations performed at the European Southern Observatory, Chile under ESO Program 078.D-0295(A).

2. Observations

2.1. Instrumental setup: the BURST mode of VISIR

We used the VISIR instrument (Lagage et al. 2004), installed at the Cassegrain focus of the Melipal telescope (UT3) of the VLT (Paranal, Chile). VISIR is a mid-IR imager that also provides a slit spectrometer. Under standard conditions at Paranal (median seeing of 0.″8 at 0.5 μm), the 8 m telescope is not diffraction-limited in the mid-IR (seeing ≈0.″4 vs. 0.″3 diffraction). Instead of a pure Airy diffraction pattern, several moving speckles and a tip-tilt usually degrade the quality of the image (e.g., Tokovinin et al. 2007). To overcome this limitation, a specific mode of the instrument called the BURST mode was introduced by Doucet et al. (2007). Its principle is to acquire very short exposures ($\Delta t \lesssim$ 50 ms), to keep the complete integration within a fraction of the coherence time (≈300 ms at Paranal in the mid-IR). The detector is therefore read very quickly, and the resulting images freeze the turbulence. It is subsequently possible to select the best images presenting a single speckle ("lucky imaging"), so they are diffraction-limited. The details of this selection procedure are given in Sect. 2.3.

2.2. Observations log

We observed MWC 300 during the first half of the night of October 3–4, 2006. A series of BURST mode observations of this star and its main PSF calibrator η Ser (HD 168723, spectral type K0III-IV) was obtained in the *PAH2* filter, whose central

Table 1. Log of the VISIR observations of MWC 300 and its main (PSF1: η Ser) and secondary (PSF2: α Eri) PSF calibrators.

#	MJD[1]	Star	DIT[2]	N exp.[3]	θ (″)[4]	AM[5]
img A	0.0044	MWC 300	10	1200 × 8	0.8	1.15
img B	0.0120	MWC 300	10	1200 × 14	1.1	1.21
img C	0.0238	MWC 300	10	1200 × 14	1.0	1.24
PSF1	0.0451	η Ser	10	1200 × 14	1.0	1.46
PSF2	0.1877	α Eri	20	1200 × 14	0.8	1.21

[1] Modified Julian date of the middle of the exposures on the target, minus 54 012.
[2] Detector Integration Time given in milliseconds for one frame.
[3] Number of image exposures in the form *nb. of frames per file* × *nb. of files*.
[4] Seeing in the visible (λ = 0.5 μm) as measured by the observatory DIMM sensor, in arcseconds.
[5] Average airmass of the observation.

wavelength is λ = 11.25 μm. The detailed transmission curves of this filter can be found in the VISIR instrument manual, available from the ESO web site[1].

The images were chopped and nodded in the north-south and east-west directions by offsetting the M2 mirror and the telescope to remove the fluctuating thermal background in the post-processing. The chopping and nodding amplitudes were both set to 8″ on the sky, and the periods were 4 and 90 s. The pixel scale was set to the smallest scale available on VISIR (0.075″/pixel), in order to sample the ≈0.3″ *FWHM* diffraction pattern of the telescope as well as possible. The MWC 300 observations were immediately followed by the PSF reference star, observed with the same instrumental setup. The journal of the VISIR observations is given in Table 1. During the observations, the seeing quality in the visible varied from 0.″8 to 1.″1.

The main PSF star, η Ser (PSF1), was chosen in the Cohen et al. (1999) catalogue of spectrophotometric standards for infrared wavelengths. In addition to its being a stable star, interferometric observations in the near-IR with the CHARA/FLUOR instrument (Mérand et al. 2007) confirm that η Ser is indeed single. It is also a stable star with respect to radial velocity (Hekker et al. 2006). An advantage of choosing the PSF star in the Cohen et al. (1999) catalogue is that its flux is absolutely calibrated, so it provides a convenient photometric reference for accurately estimating the absolute flux of the observed object. The PSF1 η Ser is located close to MWC 300 on the sky (3.°8), therefore at a comparable airmass. One should note that the seeing in the mid-IR varies much more slowly than in the visible, and is also much less sensitive to the airmass. Therefore, the effective seeing in the mid-IR images can be considered constant between the observations of MWC 300 and η Ser.

2.3. Raw data processing

The fluctuations of the thermal background were removed through the classical subtraction of the chopped and nodded images, to produce data cubes of about 10 000 images covering 6.″8 × 6.″8. After a precentering at the integer pixel level, the images were sorted by their maximum intensity, used as a proxy of the Strehl ratio (e.g., Born & Wolf 1999). The 40% best images of each cube were then resampled up by a factor 10 using a cubic spline interpolation, and the star image was subsequently centered using Gaussian fitting, at a precision level of a few mas (much smaller than the original pixel scale). The field of view was trimmed to 2.″25 × 2.″25 to reduce the computing time. The resulting cubes were eventually averaged to obtain the master images of MWC 300 and the PSFs used in our image analysis.

[1] http://www.eso.org/instruments/visir

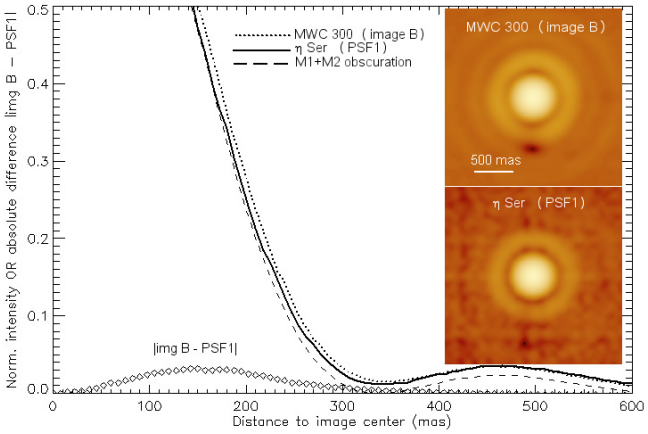

Fig. 1. Final averaged images (logarithmic scale) and normalized mean radial profile I_n of MWC 300 and PSF1 (see Table 1 for details about the observations). The MWC 300 images A and C are similar to the image B shown here. At least 3 Airy rings are well visible, specially for MWC 300. For comparison we also show the theoretical PSF profile at 11.25 μm for the VLT primary M1 mirror with central obscuration from the secondary M2 mirror. It nicely agrees with the observed PSF almost over the entire first Airy lobe. The diamonds represent the absolute difference between the radial profiles of MWC 300 and PSF1. The associated uncertainties are smaller than the symbol size, indicating that the target was partially but statistically significantly resolved by VISIR.

Table 2. Typical size of MWC 300 (2D circular Gaussian *FWHM* in units of mas) from different methods for the VISIR images A−C.

Method applied:	A	B	C	$\overline{FWHM} \pm \sigma$
Analytical estimation (Eq. (1))	70	62	57	63 ± 7
Fit of 2DCG convolved with PSF	81	72	67	73 ± 7
Richardson-Lucy deconvolution	80	68	60	69 ± 10

3. Image analysis: MWC 300 size estimation

The final averaged images of MWC 300 (image B) and of the PSF1 are shown in Fig. 1 with the corresponding normalized mean radial profiles I_n. For comparison we also give the theoretical PSF at λ = 11.25 μm for an ideal telescope with the same primary mirror (D_{VLT-M1} = 8 m) with central obscuration by the secondary mirror (D_{VLT-M2} = 1.12 m). The observed PSF is almost identical to the theoretical one over a wide range of the first Airy lobe. Moreover, the first minimum of the observed PSF is very low, reaching $I_n \simeq 0.01$. These indicate that our VISIR images are effectively diffraction-limited, at least within the first Airy lobe.

We note that the data signal-to-noise ratio (SNR) is quite high, reaching ≃2500−3500 per pixel in the core of the MWC 300 images; for the PSF1 the SNR reaches ≃1900 per pixel. Thanks to these high SNRs one can determine that the core of the MWC 300 images are statistically significantly wider than the core of the PSF, suggesting that the target was partially resolved by VISIR.

In the following we describe the different methods leading to an estimation of MWC 300's size at 11.25 μm. Main results are summarized in Table 2.

3.1. Analytical size estimation from circular Gaussians

Since MWC 300 is only slightly resolved, we first concentrate on analyzing the central peak of the images. As an initial approximation one can assume that the central peaks can be represented by a 2D circular Gaussian (hereafter 2DCG), leading to the following *FWHM* (full width at half maximum): 286.6, 284.7, 283.5 mas for the MWC 300 images A−C, and 277.8 mas for both PSFs.

Assuming that the real (deconvolved) intensity profile of MWC 300 is also represented by a 2DCG we can evaluate the angular size (*FWHM*) of MWC 300 simply from (see results from this analytical size estimation in Table 2):

$$FWHM_{\rm real} = \sqrt{FWHM^2_{\rm observed} - FWHM^2_{\rm PSF}}. \quad (1)$$

3.2. Size estimation from fit of a 2DCG convolved with PSF

In this section we apply another size estimation method that consists of fitting the MWC 300 images with a 2DCG convolved with the PSF1. This method has two advantages in comparison with the one applied in Sect. 3.1: (a) it allow us to relax the hypothesis that the central peaks of the MWC 300 and the PSF images are Gaussians, and (b) it uses not only the center of the images but also all the information available in the observed images. To perform the fit we keep, however, the assumption that the real (deconvolved) intensity distribution of MWC 300 is given by a 2DCG profile. The sizes derived from this method are also given in Table 2, where we can see that they are somewhat larger but of the same order of those obtained in the previous section.

3.3. Image deconvolution

The latter method applied was a deconvolution of the MWC 300 images by the PSF1. The only assumption about MWC 300 adopted for the deconvolution is that it has a positive intensity distribution, i.e., the positivity criterion commonly used in image processing.

We thus performed a Richardson-Lucy deconvolution using the software package Airy[2] (Correia et al. 2002) version 4.0, developed within the CAOS problem-solving environment. The size of the deconvolved images diminishes regularly at each iteration, reaching a plateau after a few hundred iterations. To estimate the size of the deconvolved images and more easily compare it with the sizes from the other methods, we fitted a 2DCG to measure the corresponding *FWHM* after each iteration. Figure 2 shows the *FWHM* of the MWC 300 deconvolved images as function of the deconvolution iteration.

The deconvolution process was repeated until 1000 iterations to make sure that the *FWHM* of the deconvolved images converged to a minimum or a plateau in our case. We present in Table 2 the average *FWHM* calculated on the central peak of the deconvolved images at the plateau regime. This plateau regime is considered to have been reached when the *FWHM* varies by less than 0.2% between two iterations. The final results do not strongly depend on this value.

The sizes obtained from deconvolution are compatible with the first two methods, especially with those from the fit of a 2DCG convolved with the PSF. As an example of a deconvolved image, we also show in Fig. 2 the average of images A−C of MWC 300 deconvolved by the PSF1 at iteration 1000. The more intense secondary structures in the deconvolved image are residuals from the first Airy ring, probably caused by the fact that the SNR of the MWC 300 images is larger than for the PSF.

[2] Available at http://fizeau.unice.fr/caos/

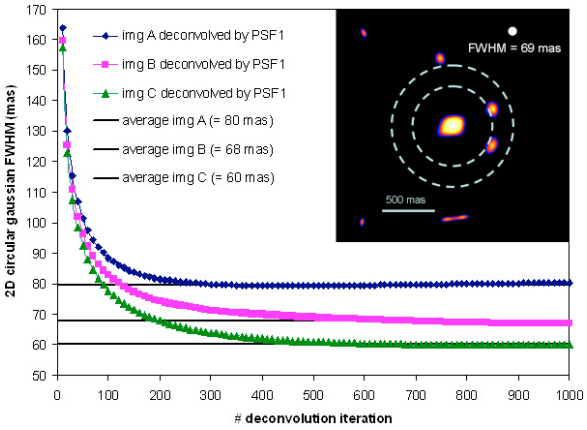

Fig. 2. *FWHM* from a fit of a 2DCG to the center of each deconvolved image of MWC 300 as a function of the iteration number. After a few hundred iterations, the MWC 300 deconvolved images converge to an almost constant *FWHM*. The average *FWHM* of each MWC 300 deconvolved image calculated on the plateau regime is compatible with the estimations from other methods (Table 2). The upper right image shows the average of images A−C deconvolved by the PSF1 at iteration 1000 (log. scale). The dashed rings indicate the first Airy ring region. The 2DCG *FWHM* from the deconvolution method is indicated.

3.4. Critical discussion on the results

To compare the results from the different methods, we show the average and corresponding standard deviation from the three MWC 300 images for a given method in Table 2. These averages and uncertainties indicate that the sizes estimated with the three different methods are in good agreement. Since the deconvolution does not impose any a priori assumption on MWC 300, we chose the average size and uncertainty from this method as the more realistic size estimation from the VISIR data: *FWHM* = 69 ± 10 mas.

To check the validity and the presence of any spurious effect on the PSF1, we also analyzed the MWC 300 images using the PSF2 (α Eri). This PSF was obtained a few hours later than MWC 300, with a different DIT, but in similar conditions of seeing and airmass (Table 1). The sizes estimated from the PSF2 completely agree with those obtained with the PSF1, giving almost identical values as in Table 2.

Because VISIR only slightly resolves MWC 300, we found it useful to check whether the resampling and shift-and-add procedures introduce any degradation in the estimated image sizes or not. We thus fitted a 2DCG to the center of each individual frame obtained after chopping and nodding correction, but before any image resampling and adding. Because these individual frames have a lower SNR than the final averaged images, we selected only the best 20% individual frames (from Strehl considerations). Figure 3 shows a histogram of *FWHM* derived from these selected individual frames. The distributions clearly show that the *FWHM* of MWC 300 frames tend to be larger than for the two PSFs. Selections with distinct percentages give similar results, but for less severe selections, the influence of atmospheric turbulence on each frame becomes stronger and stronger. Applying Eq. (1) to the maximum or median *FWHM* of these histograms results in sizes compatible with the values in Table 2.

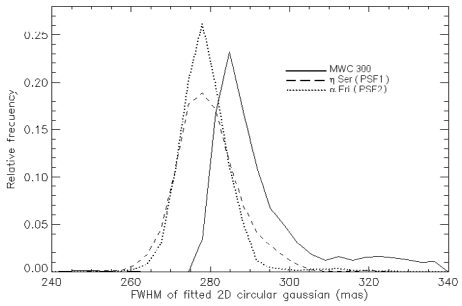

Fig. 3. Relative frequency histograms of *FWHM* obtained from a 2DCG fit to each individual frame (20% with best Strehl) after chopping and nodding correction. The PSFs have similar histograms, while the *FWHM* distribution for MWC 300 is shifted to the right, pointing to slightly wider images for the target.

4. Physical discussion and conclusions

From the VISIR observations and from the absolute flux calibration of η Ser given by Cohen et al. (1999), we estimated the flux of MWC 300 at 11.25 μm to be 84.5 ± 1.4 Jy = (20.0 ± 0.3) × 10^{-13} W/m^2/μm. This value is in good agreement with other measured fluxes in the mid-IR: for example M04 found 76.5 Jy at 10.79 μm, and the MSX observations give 70.0 Jy at 8.28 μm and 93.6 Jy at 12.13 μm (Egan et al. 2003).

From our angular size estimation (*FWHM* = 69 ± 10 mas from the deconvolution), the linear *FWHM* of MWC 300 at 11.25 μm is $FWHM_{\rm linear}$ = 125 ± 18 AU = (1.87 ± 0.26) × 10^{13} m (assuming a distance d = 1.8 kpc given by M04). For a central star radius R_* = 29 $R_\odot$, from M04, we have $FWHM_{\rm linear}$ = 924 ± 131 R_*.

Our mid-IR size is compatible with the size of the nearly edge-on model calculated by M04. The dust sublimation radius derived by them (R_1 = 147 R_*) is consistent with our measured $\mathrm{HWHM_{linear}} \equiv 0.5 * FWHM_{\rm linear}$ = 462 ± 65 R_*, since these observations impose an upper limit on the inner dust radius. Also in agreement with M04, our results provide direct support for excluding their spherical dusty model, since this model results in an object too extended: angular diameter of hottest dust shell ≃400 mas (≫*FWHM*).

For a more quantitative analysis of our size estimation, we computed a model dusty disc with the help of a Monte Carlo continuum radiative transfer code (Niccolini & Alcolea 2006). The model input parameters are those of M04, except for the mass of the disc (M = 0.01 $M_\odot$) and for the density profile, which in our case is given by a Gaussian law from R_1 = 147 R_* to 3450 R_*, followed by a $\rho \propto r^{-4}$ power-law. The synthetic image at 11.25 μm, shown in Fig. 4, well agrees with the measured VISIR *FWHM*. Figure 4 also shows that our disc model reproduces quite well the observed SED, which was obtained from the literature data. The observed SED was corrected for interstellar reddening by considering A_V = 3.76 mag, R_V = 3.1 (M04), and the analytic expressions from Cardelli et al. (1989). The adopted model gives dust temperatures above ∼600 K within the measured *FWHM*.

VISIR opens the possibility of obtaining diffraction-limited images in the mid-IR, allowing the measurement of sizes down to ≃50−100 mas. Thanks to this, the hot dust envelope size of MWC 300 has been measured for the first time. This result provides direct support to previous works suggesting the presence of a nearly edge-on dusty disc around this B[e] star. However, the VISIR images did not allow us to identify any structure of the disc, such as its elongation or inner radius. Observations at higher angular resolutions, notably with mid-IR interferometry, are required for a deeper study of the MWC 300 circumstellar environment.

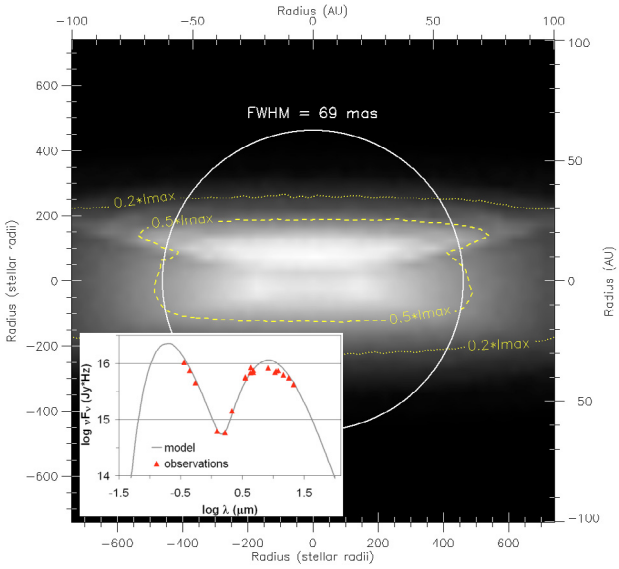

Fig. 4. Image of MWC 300 calculated with a Monte Carlo radiative transfer code (Niccolini & Alcolea 2006, see text for details). This 11.25 μm image corresponds to a nearly equator-on disc (inclination of the polar axis to the line of sight is 80°). Note that the size of the image at half intensity (dashed contour) agrees with the *FWHM* size measured with VISIR (circle). The SED for this model (inset plot) reproduces well the observed de-reddened SED for MWC 300 (triangles). The observed SED was compiled from this work (PAH2 filter) and the data in the literature: Wolf & Stahl (1985; *UBV*), Skrutskie et al. (2006; 2MASS *JHK*), Bouchet & Swings (1982; LM), M04 (NQ_s), Egan et al. (2003; MSX B1B2ACDE).

Acknowledgements. We wish to thank the VISIR instrument team at Paranal, and in particular Dr. L. Vanzi, for making the BURST mode available to us in visitor mode on very short notice. This research used the SIMBAD and VIZIER databases at the CDS, Strasbourg (France), and NASA's ADS bibliographic services. We also thank Dr. M. Carbillet for his help with the CAOS/Airy deconvolution package. The authors acknowledge the referee (Dr. A. S. Miroshnichenko) for his very useful comments and suggestions.

References

Born, M., & Wolf, E. 1999, Principles of Optics, 7th edn. (Cambridge, England: Cambridge University Press)
Bouchet, P., & Swings, J. P. 1982, Be Stars IAUS, 98, 241
Cardelli, J. A., Clayton, G. C., & Mathis, J. S. 1989, ApJ, 345, 245
Cohen, M., Walker, R. G., Carter, B., et al. 1999, AJ, 117, 1864
Correia, S., Carbillet, M., Boccacci, P., et al. 2002, A&A, 387, 733
Domiciano de Souza, A., Driebe, T., Chesneau, O., et al. 2007, A&A, 464, 81
Doucet, C., Habart, E., Pantin, E., et al. 2007, A&A, 470, 625
Egan, M. P., Price, S. D., Kraemer, K. E., et al. 2003, The Midcourse Space Experiment Point Source Catalog Version 2.3, AFRL-VS-TR-2003-1589
Hekker, S., Reffert, S., Quirrenbach, A., et al. 2006, A&A, 454, 943
Lagage, P. O., Pel, J. W., Authier, M., et al. 2004, The ESO Messenger, 117, 12
Lamers, H. J. G. L. M., Zickgraf, F.-J., de Winter, D., et al. 1998, A&A, 340, 117
Mérand, A., et al. 2007, in preparation
Miroshnichenko, A. S., Levato, H., Bjorkman, K. S., et al. 2004, A&A, 417, 731
Niccolini, G., & Alcolea, J. 2006, A&A, 456, 1
Poncelet, A., Doucet, C., Perrin, G., et al. 2007, A&A, 472, 823
Skrutskie, M. F., Cutri, R. M., Stiening, R., et al. 2006, AJ, 131, 1163
Tokovinin, A., Sarazin, M., & Smette, A. 2007, MNRAS, 378, 701
Wolf, B., & Stahl, O. 1985, A&A, 148, 412